The American Journal of Human Genetics, Volume *112*

Supplemental information

Bi-allelic variants in *MRPL49* cause variable clinical presentations, including sensorineural hearing loss, leukodystrophy, and ovarian insufficiency

Huw B. Thomas, Leigh A.M. Demain, Alfredo Cabrera-Orefice, Isabelle Schrauwen, Hanan E. Shamseldin, Alessandro Rea, Thashi Bharadwaj, Thomas B. Smith, Monika Oláhová, Kyle Thompson, Langping He, Namanpreet Kaur, Anju Shukla, Musaad Abukhalid, Muhammad Ansar, Sakina Rehman, Saima Riazuddin, Firdous Abdulwahab, Janine M. Smith, Zornitza Stark, Hanifenur Mancilar, Sait Tumer, Fatma N. Esen, Eyyup Uctepe, Vehap Topcu, Ahmet Yesilyurt, Erum Afzal, Mehri Salari, Christopher Carroll, Giovanni Zifarelli, Peter Bauer, Deniz Kor, Fatma D. Bulut, Henry Houlden, Reza Maroofian, Samantha Carrera, Wyatt W. Yue, Kevin J. Munro, Fowzan S. Alkuraya, Peter Jamieson, Zubair M. Ahmed, Suzanne M. Leal, Robert W. Taylor, Ilka Wittig, Raymond T. O'Keefe, and William G. Newman

Supplemental Data

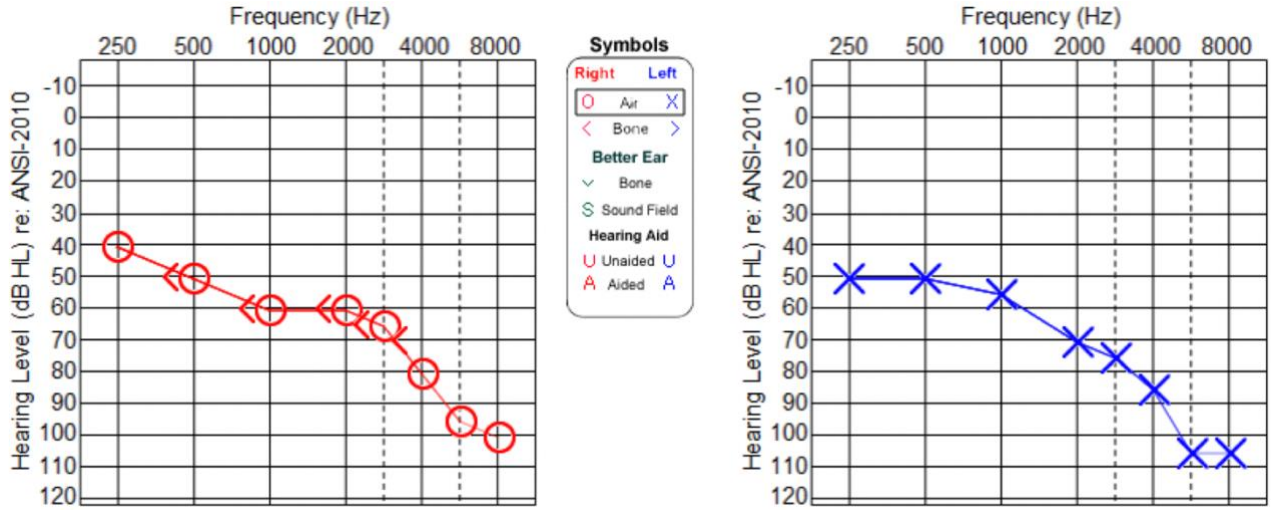

Figure S1: Audiogram for individual F1:II-1 at 16 years of age. Measurements reveal a bilateral reduction in hearing levels with increasing frequencies. Measurements for right ear indicated by red circles and left ear indicated by blue crosses.

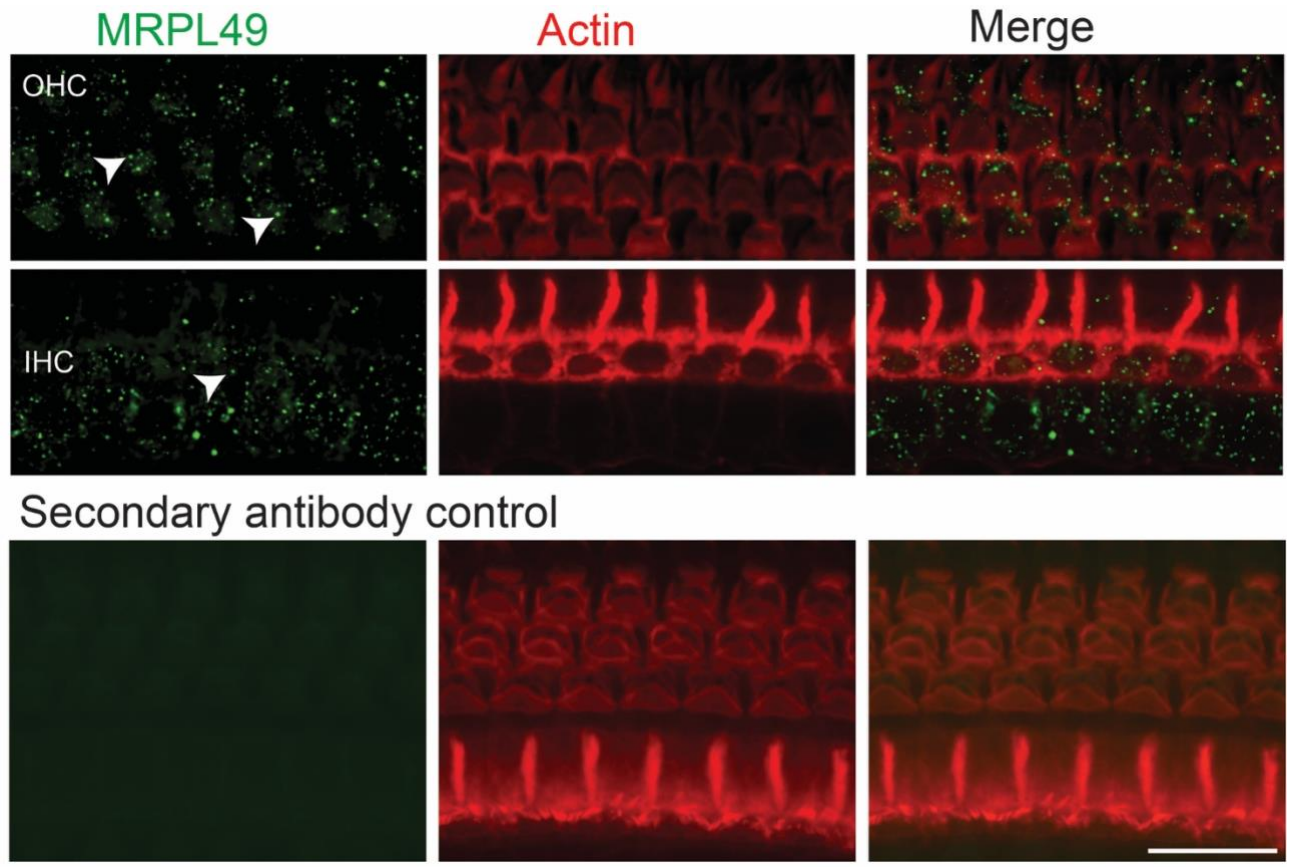

Figure S2: Whole mount immunostaining of MRPL49 in P12 wildtype mice. Immunofluorescence of mouse inner ear demonstrated that MRPL49 was localized to mitochondria indicated by arrowheads in outer hair cells (OHC), inner hair cells (IHC) and supporting cells. Scale bar, 20µm.

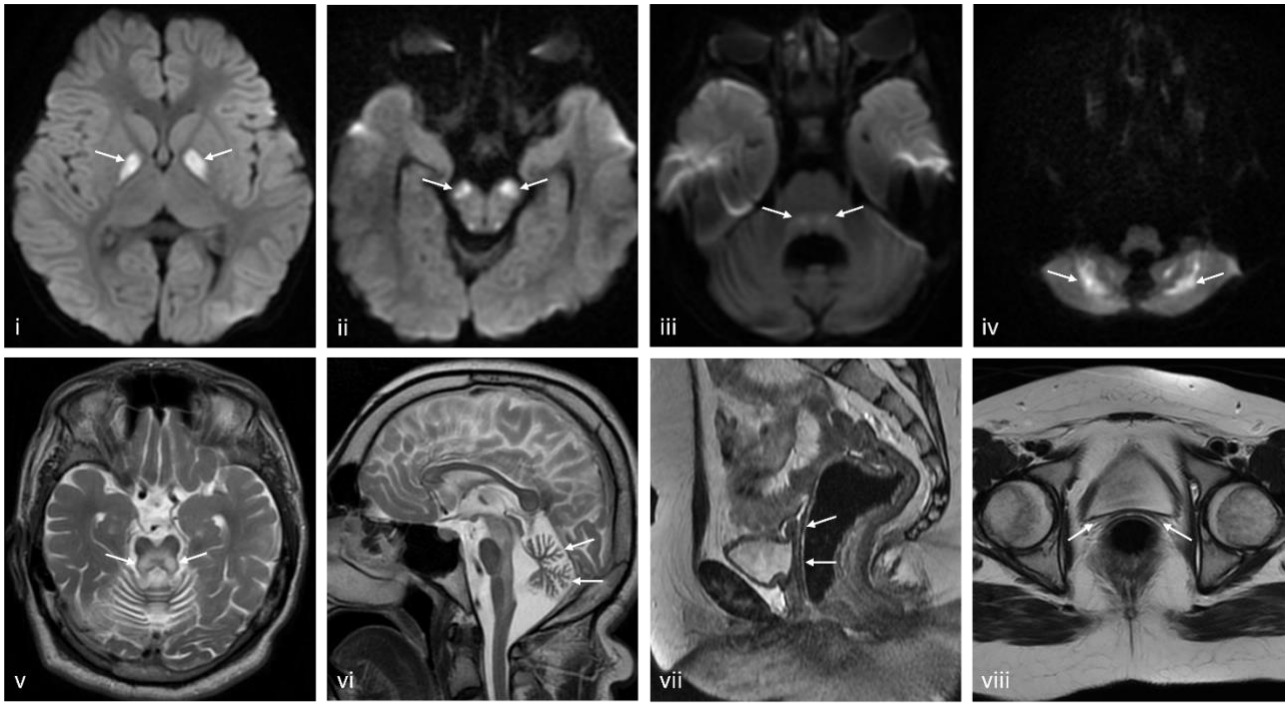

F**igure S3: Further selected MR images.** B1000 diffusion weighted images demonstrate symmetrical diffusion restriction in the globus pallidi (i), substantia nigra (ii), dorsal brainstem (iii) and cerebellum (iv). Selected T2 axial and sagittal images demonstrate dorsal brainstem T2 high signal (v), cerebellar atrophy (vi) and absence of the vagina, uterus and ovaries (vii & viii).

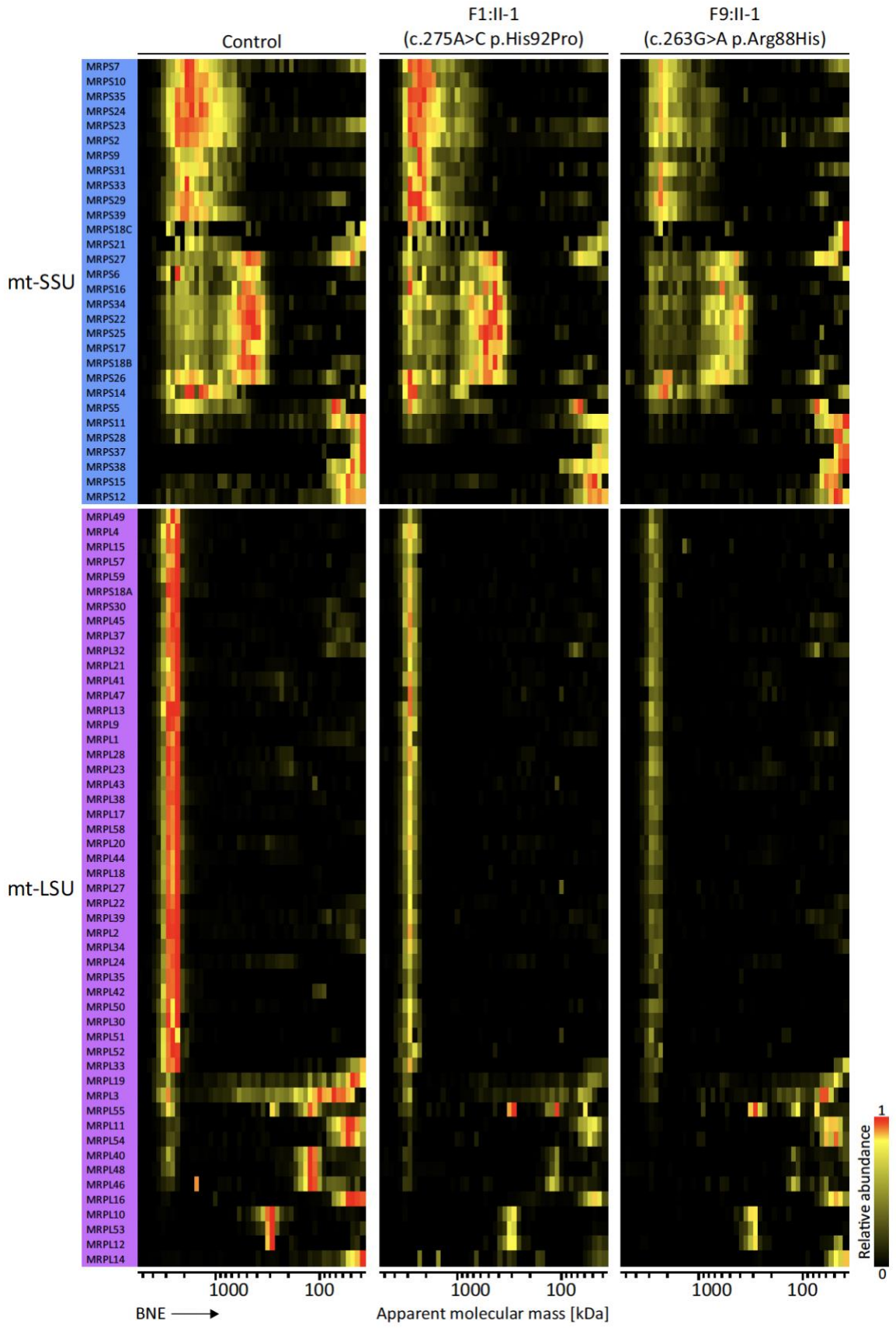

Figure S4: Expanded complexome profiles of all mitoribosome protein components identified by MS. Mitochondrial proteins were separated by BNE followed by quantitative

mass spectrometry analysis. The iBAQ values of each subunit were normalized using their maximal values across profiles. Resultant relative abundance profiles are shown as heatmaps. Maximum appearance in red, up to 50% in yellow, black indicates that protein abundance is very low, or peptides were not identified in the respective fractions. Mitoribosomal small (mt-SSU) and large (mt-LSU) subunits.

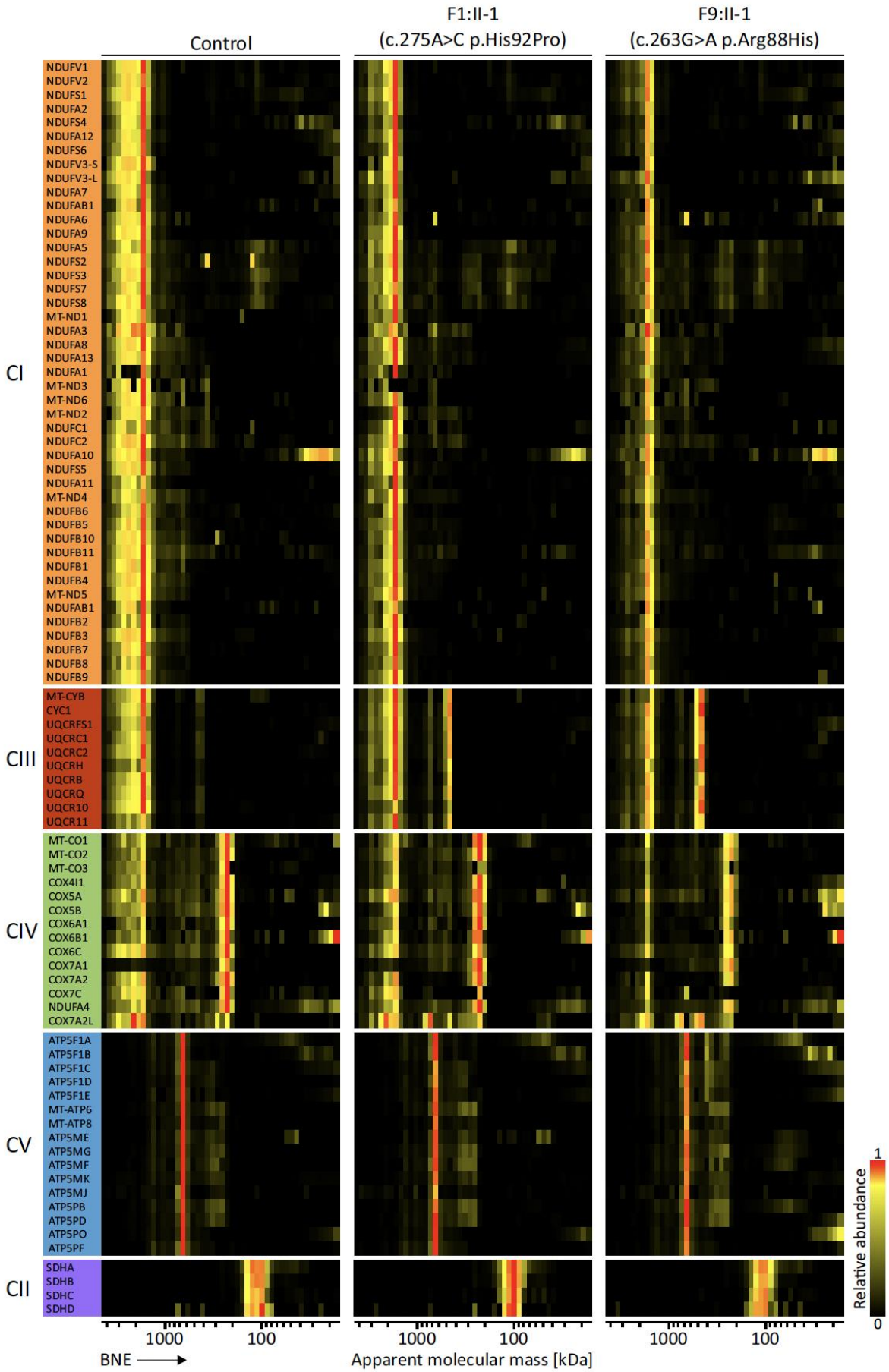
Control
F1:II-1
(c.275A>C p.His92Pro)
F9:II-1
(c.263G>A p.Arg88His)
CI
NDUFV1
NDUFV2
NDUFS1
NDUFA2
NDUFS4
NDUFA12
NDUFS6
NDUFV3-S
NDUFV3-L
NDUFA7
NDUFAB1
NDUFA6
NDUFA9
NDUFA5
NDUFS2
NDUFS3
NDUFS7
NDUFS8
MT-ND1
NDUFA3
NDUFA8
NDUFA13
NDUFA1
MT-ND3
MT-ND6
MT-ND2
NDUFC1
NDUFC2
NDUFA10
NDUFS5
NDUFA11
MT-ND4
NDUFB6
NDUFB5
NDUFB10
NDUFB11
NDUFB1
NDUFB4
MT-ND5
NDUFAB1
NDUFB2
NDUFB3
NDUFB7
NDUFB8
NDUFB9
CIII
MT-CYB
CYC1
UQCRFS1
UQCRC1
UQCRC2
UQCRH
UQCRB
UQCRQ
UQCR10
UQCR11
CIV
MT-CO1
MT-CO2
MT-CO3
COX4I1
COX5A
COX5B
COX6A1
COX6B1
COX6C
COX7A1
COX7A2
COX7C
NDUFA4
COX7A2L
CV
ATP5F1A
ATP5F1B
ATP5F1C
ATP5F1D
ATP5F1E
MT-ATP6
MT-ATP8
ATP5ME
ATP5MG
ATP5MF
ATP5MK
ATP5MJ
ATP5PB
ATP5PD
ATP5PO
ATP5PF
CII
SDHA
SDHB
SDHC
SDHD
1000
100
1000
100
1000
100
BNE
Apparent molecular mass [kDa]
Relative abundance
1
0

Figure S5: Expanded complexome profiles of all OXPHOS individual subunits identified by MS. Mitochondrial proteins were separated by BNE followed by quantitative mass spectrometry analysis. The iBAQ values of each subunit were normalized using their maximal values across profiles. Resultant relative abundance profiles are shown as heatmaps. Maximum appearance in red, up to 50% in yellow, black indicates that protein abundance is very low, or peptides were not identified in the respective fractions. CI, CII, CIII, CIV and CV stand for complexes I, II, III, IV and V, respectively.

Gene (alternative name)	Length (aa)	MIM Gene Reference	Phenotype	MIM Phenotype Reference	No. of families/variants	Ref
MRPL1	**325**	611821	-	-	-	-
MRPL2 (MRP-L14) (UL2m)	**305**	611822	-	-	-	-
MRPL3	**348**	607118	COXPD9, Cardio myopathy, SNHL, Leigh Syndrome,	614582	Multiple	[1–3]
MRPL4	**311**	611823	-	-	-	-
MRPL9	**267**	611824	-	-	-	-
MRPL10	**261**	611825	-	-	-	-
MRPL11	**192**	611826	-	-	-	-
MRPL12	**198**	602375	COXPD45	618951	One	[4]
MRPL13	**178**	610200	-	-	-	-
MRPL14	**145**	611827	-	-	-	-
MRPL15	**296**	611828	-	-	-	-
MRPL16	**251**	611829	-	-	-	-
MRPL17	**175**	611830	-	-	-	-
MRPL18	**180**	611831	-	-	-	-
MRPL19	**292**	611832	-	-	-	-
MRPL20	**149**	611833	-	-	-	-
MRPL21	**205**	611834	-	-	-	-
MRPL22	**206**	611835	-	-	-	-
MRPL23	**153**	600789	-	-	-	-
MRPL24	**216**	611836	Cerebellar atrophy, choreoathetosis of limbs and face, intellectual disability, complex I and IV defect	-	One	[5]
MRPL27	**148**	611837	-	-	-	-
MRPL28	**256**	604853	-	-	-	-
MRPL30	**161**	611838	-	-	-	-
MRPL32	**188**	611839	-	-	-	-
MRPL33	**65**	610059	-	-	-	-
MRPL34	**92**	611840	-	-	-	-
MRPL35	**188**	611841	-	-	-	-
MRPL36	**103**	611842	-	-	-	-

MRPL37	**423**	611843	-	-	-	-
MRPL38	**380**	611844	-	-	-	-
MRPL39 (MRP-L5)	**338**	611845	Early onset mitochondrial disorder	-	Multiple	[6]
MRPL40	**206**	605089	-	-	-	-
MRPL41	**137**	611846	-	-	-	-
MRPL42	**142**	611847	-	-	-	-
MRPL43	**215**	611848	-	-	-	-
MRPL44	**332**	611849	Infantile hypertrophic cardiomyopathy COXPD16	615395	Multiple	[7–10]
MRPL45	**306**	611850	-	-	-	-
MRPL46	**279**	611851	-	-	-	-
MRPL47	**250**	611852	-	-	-	-
MRPL48	**212**	611853	-	-	-	-
MRPL49	**166**	606866	Leukodystrophy, POI, SNHL, COXPD	-	Multiple	This report
MRPL50	**158**	611854	POI, SNHL, Heart dysfunction	-	One	[11]
MRPL51	**128**	611855	-	-	-	-
MRPL52	**123**	611856	-	-	-	-
MRPL53	**112**	611857	-	-	-	-
MRPL54	**138**	611858	-	-	-	-
MRPL55	**128**	611859	-	-	-	-
MRPL57 (MRP63)	**102**	611997	-	-	-	-
MRPL58	**206**	603000	-	-	-	-
MRPL59 (GADD45GIP1/ML64)	**222**	605162	-	-	-	-

Table S1: Table listing mt-LSU proteins and their associated disorders

Variant	c.125_126delTG p.Val42Glyfs*2	c.262C>T p.Arg88Cys	c.263G>A p.Arg88His	c.275A>C p.His92Pro
Allele count	97/1614050	49/1613940	6/1614036	25/1614092
Allele frequency	6.01e-5	3.04e-5	3.72e-6	1.55e-5
Number of homozygotes	0	0	0	0

Table S2: *MRPL49* variant allele frequencies in gnomAD v4.0 (accessed 7/8/24)

	c.262C>T p.Arg88Cys	c.263G>A p.Arg88His	c.275A>C p.His92Pro	c.125_126delTG p.Val42GlyfsTer2
Location (hg38)	Chr 11:65125520C>T	Chr 11:65125521G>A	Chr 11:65125533A>C	Chr 11:65124546TG
dbSNP	rs758327244	rs1565337413	rs770118409	rs751218133
SIFT	Deleterious (0.01)	Deleterious (0)	Deleterious (0)	-
PolyPhen	Benign (0.338)	Probably damaging (0.988)	Probably damaging (0.993)	-
CADD	25.2	27.1	25.2	24.2
Mutation taster	Disease causing (0.999)	Disease causing (0.999)	Disease causing (0.999)	Disease causing (1)

Table S3:
In silico pathogenicity predictions for *MRPL49* variants identified in this study

Target	Forward sequence 5'-3'	Reverse sequence 5'-3'
MT-RNR1 (12s)	TAGAGGAGCCTGTTCTGTAATCGAT	CGACCCTTAAGTTTCATAAGGGCTA
MT-RNR2 (16s)	GCCTGCCCAGTGACACATG	CACGGGCAGGTCAATTTCAC
MRPL49 (Exon 3)	TGGCCCTCTGCAGACTGAGAGC	AGGTCAGGCCAAGAGTCC
MRPL49 (qPCR)	CCGGCTACCAGGATCCCAG	CGGATCACAGTCATCTGCCG
ACTB	GTGGATCAGCAAGCAGGAGT	GTAACAACGCATCTCATATTTGGAA

Table S4:
Primer sequences used during the study

Supplemental Methods:

Fibroblast cell culture

Fibroblast cells were cultured in high glucose Dulbecco's Modified Eagle's Medium (Merck) supplemented with 10% (v/v) foetal calf serum (Gibco) and 100U/ml penicillin, 100ug/ml streptomycin, at 37°C with 5% CO_2 or supplemented with 10% fetal calf serum, 1× non-essential amino acids, 50 U/ml penicillin, 50 µg/ml streptomycin and 50 µg/ml uridine.

SDS-PAGE and Immunoblotting

Cells were lysed in RIPA buffer (Sigma) supplemented with protease inhibitor cocktail (Promega), gently agitated at 4°C for 30 minutes and centrifuged at 13,000 rpm for 15 mins. Samples were mixed with SDS-PAGE sample buffer, loaded onto a 12% polyacrylamide gel and run at 180V for up to 90 mins. Proteins were transferred onto a 0.45um PVDF blotting membrane (GE Healthcare) by semi-dry transfer (20V for 30 minutes) before being blocked with TBS-Tween + 5% dried milk power. Primary antibodies specific to each of the mitochondrial respiratory chain complexes as provided by the Total OXPHOS Human WB Antibody Cocktail (ATP5A, UQCRC2, SDHB, COXII, and NDUFB8) (Abcam, ab110411) and Beta-actin (Proteintech; 20536-1-AP, 66009-1-Ig) were incubated overnight at 4°C. Dilutions were 1:500 (OXPHOS cocktail) and 1:5000 (Beta-actin). Membranes were subsequently washed and incubated at room temperature for 90 minutes with either IRDye 680RD Goat anti-Mouse IgG antibody (LI-COR, 926-68070), or IRDye. 800CW Goat anti-Rabbit IgG (LI-COR, 926-32211). Membranes were finally imaged and quantified using the LICOR Odyssey FC imaging system.

DNA/RNA extraction

DNA was extracted from patient and control fibroblasts using the DNA minikit following recommended manufacturer's protocols (Qiagen), DNA was subsequently stored at –80°C. RNA was extracted from patient and control fibroblasts using Tri-Reagent ® (Merck) following manufacturer's protocol. RNA was further purified by RNeasy column cleanup (Qiagen) which included an on-column DNase digest step. Purified RNA was immediately used for cDNA synthesis and/or snap frozen at -80°C for storage.
cDNA synthesis: cDNA was generated from purified RNA using GoScript first strand synthesis protocol (NEB) using random hexamer primers (Thermo Fisher Scientific).

RT-qPCR

Quantification of patient and control cDNA was performed using PowerUp SYBR Green mastermix (Thermo Fisher) and gene specific primers listed in Table S4. For each separate experiment the mean of triplicate measurements was normalized to ACTB as a housekeeping control.

Sanger sequencing

For variant validation in patient fibroblasts, Exon 3 of *MRPL49* was amplified via RT-PCR using "MRPL49 (Exon 3)" primers listed in supplemental table S4. The resulting PCR product was run on a 1% agarose gel, extracted and purified before being prepared for Sanger sequencing. Sanger sequencing was performed by Eurofins Genomics.

Mitochondrial enzyme activity assay

Assessment of mitochondrial respiratory chain enzymes in fibroblasts from affected individuals (F1:II-1 and F9:II-1) was performed as previously described[12]

Complexome analysis

Cells were homogenized using a motor-driven glass Potter-Elvehjem homogenizer with a Teflon pestle at 2,000 RPM and 40 strokes in a cold room (4 °C). Homogenates were centrifuged for 3 min at 500 x *g* to remove nuclei, cell debris, and unbroken cells. Mitochondrial membranes were sedimented by centrifugation for 10 min at 10,000 x *g*. Protein content was determined using the DC method (Bio-Rad) and mitochondrial enriched pellets (400 µg protein) were resuspended in 40 µl solubilisation buffer (50 mM imidazole pH 7.0, 50 mM NaCl, 1 mM EDTA, 2 mM aminocaproic acid) supplemented with 12 µl 20%(m/v) digitonin (Serva) and processed as described in[13]. Equal protein amounts of samples (100 µg protein) were subjected to Blue Native electrophoresis (BNE) using a 3 to 18% polyacrylamide gradient gel (dimension 14 x 14 cm). After native electrophoresis in a cold chamber, gels were fixed in 50%(v/v) methanol, 10%(v/v) acetic acid, 10 mM ammonium acetate for 30 min and stained with Coomassie Blue dye (0.025% Serva Blue G-250 in 10%(v/v) acetic acid).

Each lane of the native gel was cut into equal fractions and collected in 96-well filter plates. The gel pieces were destained in 60% Methanol, 50 mM ammonium bicarbonate (ABC). Excess solution was removed by centrifugation for 2 min at 600 x *g*. Proteins were reduced in 10 mM DTT, 50 mM ABC for one hour at 56°C and further alkylated for 45 min in 30 mM iodoacetamide. Samples were digested in 5 ng trypsin (sequencing grade, Promega)/µl in 50 mM ABC, 10% acetonitrile (ACN), 0.01% ProteaseMAX surfactant (Promega), 1 mM $CaCl_2$ for 16 hours at 37°C. Peptides were eluted with 30% ACN and 3% formic acid (FA), centrifuged into a fresh 96-well PCR plate, dried in a SpeedVac and resolubilized in 1 % ACN, 0.5% FA and stored at -20°C until MS analysis.

The peptides (3 µl of each fraction) were analyzed by LC-MS/MS using a Q Exactive Plus Orbitrap equipped with an UHPLC Dionex Ultimate 3000 instrument (Thermo Fisher Scientific). The peptides were loaded on an Acclaim™ PepMap™ 100 C18 LC Pre-column (0.1 mm x 20 mm, nanoViper, 5 µm, 100 Å) and separated using emitter columns (15 cm length × 100 µm ID × 360 µm OD × 15 µm orifice tip; MS Wil/CoAnn Technologies) filled with ReproSilPur C18-AQ reverse-phase beads of 3 µm, 100 Å (Dr. Maisch GmbH). HPLC and MS specific details are available at the PRIDE entry. MaxQuant 2.0.3.0[14] was used to perform the proteomic search. The human reference proteome database (UniProt, December 2022, including canonical sequences, isoforms and the two MRPL49 variants) was used for identification with a false discovery rate (FDR) ≤1%. Additional search details are available at the PRIDE entry. To quantify the protein abundances, iBAQ values were calculated. The proteinGroups.txt output file was automatically processed using "process_maxquant" (https://github.com/joerivstrien/process_maxquant). The resulting dataset was manually inspected and analyzed using Microsoft Excel. The list of protein groups was hierarchically clustered based on the abundance patterns with an average linkage algorithm (absolute correlation) using Cluster 3.0[15]. Individual profiles were corrected using the sum of iBAQ values of the identified proteins annotated in MitoCarta 3.0[16] Calibration curves of apparent molecular masses were generated using human membrane and water-soluble protein

complexes of known masses. Data were normalized to the maximal iBAQ value across all slices for each protein group to generate the relative abundance profiles and visualized as heatmaps/line charts generated in Microsoft Excel. To analyze multi-protein complexes, additional profiles were generated by averaging the iBAQ values of all individual components identified by MS. Quantification of the abundance differences was done by calculating the area under the curve (AUC) of the regions of interest.

Mouse inner ear immunostaining:
Immunofluorescence of mouse inner and outer hair cells was performed as previously described[17] using an anti-MRPL49 antibody (NBP2-13618 Novus) at 1:200 dilution.

Supplemental references

1. Bursle, C., Narendra, A., Chuk, R., Cardinal, J., Justo, R., Lewis, B., and Coman, D. (2017). COXPD9 an Evolving Multisystem Disease; Congenital Lactic Acidosis, Sensorineural Hearing Loss, Hypertrophic Cardiomyopathy, Cirrhosis and Interstitial Nephritis. JIMD Rep *34*, 105–109. https://doi.org/10.1007/8904_2016_13.

2. Galmiche, L., Serre, V., Beinat, M., Assouline, Z., Lebre, A.-S., Chretien, D., Nietschke, P., Benes, V., Boddaert, N., Sidi, D., et al. (2011). Exome sequencing identifies MRPL3 mutation in mitochondrial cardiomyopathy. Hum Mutat *32*, 1225–1231. https://doi.org/10.1002/humu.21562.

3. Alsharhan, H., Muraresku, C., and Ganetzky, R.D. (2021). COXPD9 in an individual from Puerto Rico and literature review. Am J Med Genet A *185*, 2519–2525. https://doi.org/10.1002/ajmg.a.62344.

4. Serre, V., Rozanska, A., Beinat, M., Chretien, D., Boddaert, N., Munnich, A., Rötig, A., and Chrzanowska-Lightowlers, Z.M. (2013). Mutations in mitochondrial ribosomal protein MRPL12 leads to growth retardation, neurological deterioration and mitochondrial translation deficiency. Biochim Biophys Acta *1832*, 1304–1312. https://doi.org/10.1016/j.bbadis.2013.04.014.

5. Di Nottia, M., Marchese, M., Verrigni, D., Mutti, C.D., Torraco, A., Oliva, R., Fernandez-Vizarra, E., Morani, F., Trani, G., Rizza, T., et al. (2020). A homozygous MRPL24 mutation causes a complex movement disorder and affects the mitoribosome assembly. Neurobiol Dis *141*, 104880. https://doi.org/10.1016/j.nbd.2020.104880.

6. Amarasekera, S.S.C., Hock, D.H., Lake, N.J., Calvo, S.E., Grønborg, S.W., Krzesinski, E.I., Amor, D.J., Fahey, M.C., Simons, C., Wibrand, F., et al. (2023). Multi-omics identifies large mitoribosomal subunit instability caused by pathogenic MRPL39 variants as a cause of pediatric onset mitochondrial disease. Hum Mol Genet *32*, 2441–2454. https://doi.org/10.1093/hmg/ddad069.

7. Carroll, C.J., Isohanni, P., Pöyhönen, R., Euro, L., Richter, U., Brilhante, V., Götz, A., Lahtinen, T., Paetau, A., Pihko, H., et al. (2013). Whole-exome sequencing identifies a mutation in the mitochondrial ribosome protein MRPL44 to underlie mitochondrial infantile cardiomyopathy. J Med Genet *50*, 151–159. https://doi.org/10.1136/jmedgenet-2012-101375.

8. Distelmaier, F., Haack, T.B., Catarino, C.B., Gallenmüller, C., Rodenburg, R.J., Strom, T.M., Baertling, F., Meitinger, T., Mayatepek, E., Prokisch, H., et al. (2015). MRPL44 mutations cause a slowly progressive multisystem disease with childhood-onset hypertrophic cardiomyopathy. Neurogenetics *16*, 319–323. https://doi.org/10.1007/s10048-015-0444-2.

9. Friederich, M.W., Geddes, G.C., Wortmann, S.B., Punnoose, A., Wartchow, E., Knight, K.M., Prokisch, H., Creadon-Swindell, G., Mayr, J.A., and Van Hove, J.L.K. (2021). Pathogenic variants in MRPL44 cause infantile cardiomyopathy due to a mitochondrial

translation defect. Mol Genet Metab *133*, 362–371. https://doi.org/10.1016/j.ymgme.2021.06.001.

10. Horga, A., Manole, A., Mitchell, A.L., Bugiardini, E., Hargreaves, I.P., Mowafi, W., Bettencourt, C., Blakely, E.L., He, L., Polke, J.M., et al. (2021). Uniparental isodisomy of chromosome 2 causing MRPL44-related multisystem mitochondrial disease. Mol Biol Rep *48*, 2093–2104. https://doi.org/10.1007/s11033-021-06188-1.

11. Bakhshalizadeh, S., Hock, D.H., Siddall, N.A., Kline, B.L., Sreenivasan, R., Bell, K.M., Casagranda, F., Kamalanathan, S., Sahoo, J., Narayanan, N., et al. (2023). Deficiency of the mitochondrial ribosomal subunit, MRPL50, causes autosomal recessive syndromic premature ovarian insufficiency. Hum Genet *142*, 879–907. https://doi.org/10.1007/s00439-023-02563-z.

12. Frazier, A.E., Vincent, A.E., Turnbull, D.M., Thorburn, D.R., and Taylor, R.W. (2020). Assessment of mitochondrial respiratory chain enzymes in cells and tissues. Methods Cell Biol *155*, 121–156. https://doi.org/10.1016/bs.mcb.2019.11.007.

13. Wittig, I., Braun, H.-P., and Schägger, H. (2006). Blue native PAGE. Nat Protoc *1*, 418–428. https://doi.org/10.1038/nprot.2006.62.

14. Tyanova, S., Temu, T., and Cox, J. (2016). The MaxQuant computational platform for mass spectrometry-based shotgun proteomics. Nat Protoc *11*, 2301–2319. https://doi.org/10.1038/nprot.2016.136.

15. de Hoon, M.J.L., Imoto, S., Nolan, J., and Miyano, S. (2004). Open source clustering software. Bioinformatics *20*, 1453–1454. https://doi.org/10.1093/bioinformatics/bth078.

16. Rath, S., Sharma, R., Gupta, R., Ast, T., Chan, C., Durham, T.J., Goodman, R.P., Grabarek, Z., Haas, M.E., Hung, W.H.W., et al. (2021). MitoCarta3.0: an updated mitochondrial proteome now with sub-organelle localization and pathway annotations. Nucleic Acids Res *49*, D1541–D1547. https://doi.org/10.1093/nar/gkaa1011.

17. Giese, A.P.J., Tang, Y.-Q., Sinha, G.P., Bowl, M.R., Goldring, A.C., Parker, A., Freeman, M.J., Brown, S.D.M., Riazuddin, S., Fettiplace, R., et al. (2017). CIB2 interacts with TMC1 and TMC2 and is essential for mechanotransduction in auditory hair cells. Nat Commun *8*, 43. https://doi.org/10.1038/s41467-017-00061-1.